A comparative study of surface- and volume-based techniques for the automatic registration between CT and SPECT brain images

George C. Kagadis[a)]
Department of Medical Physics, School of Medicine, University of Patras, Rion, Greece

Konstantinos K. Delibasis, George K. Matsopoulos, Nikolaos A. Mouravliansky, and Pantelis A. Asvestas
Institute of Communication and Computer Systems, National Technical University of Athens, Greece

George C. Nikiforidis[b)]
Department of Medical Physics, School of Medicine, University of Patras, Rion, Greece

(Received 24 January 2001; accepted for publication 15 November 2001; published 25 January 2002)

Image registration of multimodality images is an essential task in numerous applications in three-dimensional medical image processing. Medical diagnosis can benefit from the complementary information in different modality images. Surface-based registration techniques, while still widely used, were succeeded by volume-based registration algorithms that appear to be theoretically advantageous in terms of reliability and accuracy. Several applications of such algorithms for the registration of CT–MRI, CT–PET, MRI–PET, and SPECT–MRI images have emerged in the literature, using local optimization techniques for the matching of images. Our purpose in this work is the development of automatic techniques for the registration of real CT and SPECT images, based on either surface- or volume-based algorithms. Optimization is achieved using genetic algorithms that are known for their robustness. The two techniques are compared against a well-established method, the Iterative Closest Point—ICP. The correlation coefficient was employed as an independent measure of spatial match, to produce unbiased results. The repeated measures ANOVA indicates the significant impact of the choice of registration method on the magnitude of the correlation ($F=4.968$, $p=0.0396$). The volume-based method achieves an average correlation coefficient value of 0.454 with a standard deviation of 0.0395, as opposed to an average of 0.380 with a standard deviation of 0.0603 achieved by the surface-based method and an average of 0.396 with a standard deviation equal to 0.0353 achieved by ICP. The volume-based technique performs significantly better compared to both ICP ($p<0.05$, Neuman Keuls test) and the surface-based technique ($p<0.05$, Neuman–Keuls test). Surface-based registration and ICP do not differ significantly in performance. © *2002 American Association of Physicists in Medicine.*
[DOI: 10.1118/1.1445412]

Key words: image registration, CT, SPECT, mutual information, average surface distance

INTRODUCTION

In medical imaging, registration between two-dimensional (2-D) or three-dimensional (3-D) images is a common problem encountered when more than one image of the same anatomical structure is obtained, either using different imaging modalities or performing dynamic studies. In all cases, the information present in the different images must be combined to produce fused or parametric images. Registration can be performed between two modalities with anatomical information (CT–CT or CT–MR), between anatomical atlases (a 3-D model image with certain areas clearly labeled in advance[1]) and functional studies (CT–PET, CT–SPECT, MR–PET, etc.) or between images of the same modality, taken at different times. Comprehensive surveys of medical image registration can be found in van den Elsen *et al.*[2] and Maurer *et al.*,[3] in terms of imaging modalities and employed techniques.

The process of image registration can be formulated as a problem of optimizing a function that quantifies the match between the original and the transformed image. Several image features have been used for the matching process, depending on the modalities used, the specific application, and the implementation of the geometric transformation. The registration process can be divided into three main categories: point-based, surface-based, and volume-based methods.

Point-based registration involves the determination of the coordinates of corresponding points in different images and the estimation of geometrical transformation using these corresponding points. Such points can be defined using external markers placed on the patient's skin before the acquisition,[4] stereotactic frames,[5] landmarks,[6] and the bone marker procedure, a technique that is exploiting the fact that bones and areas in the immediate vicinity can be registered by rigid transformation.[7] External markers have been used to register SPECT–MR images with the affine transformation method[8] and CT–MR data with 3-D global transformations.[9] The low resolution along the transverse axis, the small number of corresponding markers, as well as possible inaccuracies in their placement during the acquisition from each modality,

render these methods as semiautomatic resulting in inaccuracies and inconsistencies.

Surface-based registration involves the determination of surfaces of anatomical structures that exist in both images and the minimization of a distance measure between these corresponding surfaces. The surfaces are generally represented as set of large number of points obtained by segmenting contours in contiguous image slices. Certain surface-based registration techniques may require the points of the surface to be triangulated.[10] The difference between point-based and surface-based registration algorithms is that point correspondence is defined by the user for the former, whereas in automatic for the latter. Pelizzari *et al.*[11] introduced the idea of using surfaces to register brain images by obtaining a rigid body transformation, which when applied to ''hat'' coordinates (points that belong to the skin surface of the scan with the lower resolution) minimizes a residual that is the mean square distance between ''hat'' points and ''head'' surface (a stack of skin contours from the higher resolution scan) using an optimization technique described by Powell.[12] The Euclidean distance between a point of an image and the closest surface point is used in the work of Kozinska *et al.*[13] as a closest point projection rule, whereas the integer approximations of the Euclidean distance as well as its highly computation cost required were improved by using the well-known chamfer distance transform.[14] This method was then applied to medical image registration.[15,16] Besl *et al.*[17] presented a general purpose registration technique called the ''Iterative Closest Point method,'' which was extended and implemented toward medical applications.[18,19]

Volume-based registration involves the optimization of a quantity measuring the similarity of all geometrically corresponding voxel pairs, considering some predefined features. Multiple volume-based algorithms have been proposed,[20,21] optimizing a measure of the absolute difference between image intensities of corresponding voxels within overlapping parts in a region of interest. These methods were based on the assumption that the two images are linearly correlated, which is not the general case. Cross correlation of feature images derived from the original image data has been applied to CT–MR modeling using geometrical features, such as edges[22] and ridges[23,24] or using specially designed intensity transformations.[25] Misregistration was measured by the dispersion of the 2-D histogram of the image intensities of corresponding voxel pairs, which was assumed to be minimal in the registered position. Studholme *et al.*[26] criterion required segmentation of the images or delineation of specific histogram regions, while the Woods *et al.*[27] criterion was based on an additional assumption concerning relationships between the gray values in the different modalities to reduce the complexity. Collignon *et al.*[28] and Maes *et al.*[29] introduced the mutual information (MI) registration criterion, measuring the statistical dependence between two random variables or the amount of information that one variable contains about the other. The MI of the image intensity values of corresponding voxel pairs was maximal if the images were geometrically aligned. A comparative study between surface and volume-based registration algorithms was recently published by West *et al.*,[30] which indicates that the volume-based techniques tend to give more accurate and reliable results when the CT–MR images are registered, and slightly more accurate results for the PET–MR images. The reason lies with the fact that surface-based registration methods require well-defined corresponding surfaces prior to registration.

In this paper, a comparative study of two automatic registration methods is presented and applied on a number of pairs of clinical three-dimensional (3-D) CT–SPECT brain images in order to establish a usefulness method for the automatic registration of the data from these modalities. The first method is surface based and it is used to automatically register the inner skull surface of the CT with the outer brain surface from the SPECT data. The second developed technique is a volume-based one, and utilizes the MI from the two images to be registered. Both methods exploit the optimization efficiency of genetic algorithms (GAs), as a global optimization technique, combined with a local one, such as the Powell technique, in obtaining the parameters of the affine transformation for the automatic registration of CT and SPECT images. Furthermore, these two proposed automatic registration methods are compared against a well-established registration method, the Iterative Closest Point (ICP) method and their performances are validated qualitatively and quantitatively. The advantages of the volume-based registration method, as finally proposed to automatically register CT and SPECT data, include stability and repeatability of performance, speed of execution, independence of clinical protocol, and robustness due to the employed genetic algorithms as an optimization process.

For the present study we selected patients suffering from ischemia (acute–chronic–transient) and patients with subarachnoid hemorrhage.

It is well known that in brain ischemia SPECT is able to provide an early diagnosis, while CT better describes the anatomic features. Our study strengthens our belief that registering the two images gives us the opportunity to estimate more accurately the extent and the position of the lesion, resulting in a more accurate diagnosis, prognosis, and consequent treatment.

DATA ACQUISITION

X-ray CT and SPECT brain images were acquired from five (5) patients (five pairs of data) at the Radiology and Nuclear Medicine Departments of the University Hospital of Patras, Greece. CT datasets were acquired with a Somatom Plus 4 Power scanner (Siemens, Erlangen) at 120 kV and 180 mAs without administration of contrast media. Slice thickness was set to 3 mm, feed was 3 mm/s, and the region of interest was about 13 cm. Reconstruction was performed with a soft kernel algorithm and the 512×512 pixel slices with 12 bits per pixel were degraded to 128×128 for the coregistration process. Thus, a linear interpolation technique was applied to the CT data to reduce the memory require-

TABLE I. The acquisition parameters of the CT–SPECT head data used.

Matching scheme		Acquisition parameters: Pixel matrix	Slice thickness (mm)	No slices	FOV (cm)	Voxel size (mm×mm×mm)
Pair-1	CT	128×128	3	47	22.78	1.78×1.78×3
	SPECT	128×128	3	83	···	1.49×1.49×3
Pair-2	CT	128×128	1.5	42	19.07	1.49×1.49×1.5
	SPECT	128×128	1.5	80	···	1.49×1.49×1.5
Pair-3	CT	128×128	1.5	67	22.53	1.76×1.76×1.5
	SPECT	128×128	1.5	67	···	1.49×1.49×1.5
Pair-4	CT	128×128	1.5	74	19.07	1.49×1.49×1.5
	SPECT	128×128	1.5	70	···	1.49×1.49×1.5
Pair-5	CT	128×128	3	42	21.63	1.69×1.69×3
	SPECT	128×128	3	48	···	1.40×14.40×3

ments and the total execution time for the registration process.[31] There was no slice spacing or slice overlap for all CT datasets.

While patients laid in a dimly lit quiet room, with their eyes open, an intravenous dose (703–777 MBq) of ^{99m}Tc-ethyl cysteinate dimmer (ECD) (Neurolite, DuPont Merck Pharmaceuticals, Billerica, MA) was administered.[32,33] Forty-five minutes after ECD injection brain perfusion acquisition was performed at 6° increments on a dual-head gamma camera system with low-energy, general-purpose collimators (Elscint Helix, Israel). Post acquisition, intrinsic Metz postfiltering and finally attenuation correction based on Chang's iterative method[34] were serially applied. In the attenuation correction step the body contour of the SPECT data is assumed to be an ellipse, and the weight given for each point inside the ellipse is calculated according to Chang's formula. Points outside the ellipse have a correction value of 0. The calculation of Chang's integral is done by a discrete computation. Each reconstructed slice contains 128×128 pixels, using 8 bits per pixel, with no slice spacing for each SPECT dataset. The acquisition parameters of the data used in this paper, along with the corresponding FOV of the CT data, are listed in Table I. As it can be seen, the FOV was not the same for all CT data sets since its value was set according to the pathology of the subjects, during the acquisition process. The voxel size is given in mm in Table I along the *x* and *y* axes, whereas the size along the *z* axis is defined as the sum of the slice thickness. The intrinsic spatial resolution for the first head of the gamma camera is 3.72 mm while for the second head is 3.78 mm.

Both the gamma camera and the CT scanner are checked regularly with the quality control processes described in AAPM Reports No. 6, No. 22 and No. 39.[35–37]

METHODOLOGY

The methodology of two proposed automatic registration methods is diagrammatically presented in Fig. 1, where the following steps are presented: preprocessing step (depending on the method), selection of a measure of spatial match between the images to be registered (depending on the method), selection of a geometric transformation model (common for both methods), and selection of an optimization technique for the determination of transformation parameters (common for both methods).

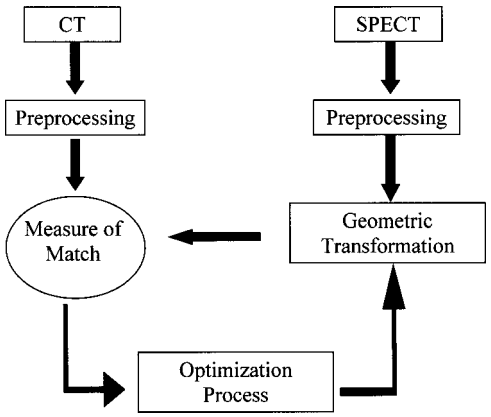

FIG. 1. Typical diagram of the proposed automatic registration methods.

Preprocessing of CT and SPECT brain images

Surface-based automatic registration: In the case of the pair of CT and SPECT brain images, a match has to be achieved between the inner skull CT surface and the outer SPECT brain surface. Since the SPECT data have been acquired from a cerebral perfusion study, at which no concentration of radioactive material occurs at the bone structures, these two surfaces are the closest possible match for the given modalities.

A prerequisite for the proposed CT–SPECT automatic registration scheme is the extraction of the voxels of the common surfaces from the two images. Different approaches were followed for the CT and the SPECT data. For the CT data, the inner skull surface's voxels are obtained using morphological operations,[38] according to the following equation:

$$V_{CT}=[T(X)\circ B_1]\cap\{[T(X)\circ B_1]\otimes B_2\}^C, \quad (1)$$

where V_{CT} are the inner skull CT surface's voxels, X is the original CT data, $T(X)$ is the threshold operator that produces a binary output such that voxels with original values greater than the threshold level obtain values equal to 1, and $\circ$ is the symbol for the opening operation (erosion followed by a dilation) using the circular disk B_1 with a diameter of 21 pixels, as a structuring element, and $\otimes$ is the symbol of the erosion operation using a rectangular structuring element, B_2, with size 3×3. The opening operation removes any background and the skull information while it restores the CT inner area, in a binary format, to its original size. The superscript C denotes the complement of the set $\{[T(X)\circ B_1 \otimes B_2]\}$ with respect to the set $[T(X)\circ B_1]$. Finally, the intersection, $\cap$, produces the inner CT skull surface. The proposed method is fast and robust since the aforementioned approach does not require any user intervention.

For the SPECT data, the outer surface's voxels, V_{SPECT}, are obtained according to the following equation:

$$V_{SPECT}=T(X)\cap[T(X)\otimes B_2]^C, \quad (2)$$

where the same notation is used as in Eq. (1). A simple thresholding T belonging to the range between 5–25 pixels was employed. The value of the aforementioned threshold operation does not vary substantially between different SPECT images.

A coarse registration is initially achieved by translating the points of the SPECT surface so that their center of mass coincides with CT-surface's center of mass and then scaling the SPECT surface points coordinates to compensate for the difference of voxel size between the two modalities. Equation (3) demonstrates the above process:

$$\begin{bmatrix} x' \\ y' \\ z' \end{bmatrix}_{\text{SPECT}} = \begin{bmatrix} \frac{V_x^{\text{SPECT}}}{V_x^{\text{CT}}} & 0 & 0 \\ 0 & \frac{V_y^{\text{SPECT}}}{V_y^{\text{CT}}} & 0 \\ 0 & 0 & \frac{V_z^{\text{SPECT}}}{V_z^{\text{CT}}} \end{bmatrix} \times \begin{bmatrix} x_{\text{SPECT}} + (\overline{x}_{\text{CT}} - \overline{x}_{\text{SPECT}}) \\ y_{\text{SPECT}} + (\overline{y}_{\text{CT}} - \overline{y}_{\text{SPECT}}) \\ z_{\text{SPECT}} + (\overline{z}_{\text{CT}} - \overline{z}_{\text{SPECT}}) \end{bmatrix}, \tag{3}$$

where $(x',y',z')_{\text{SPECT}}$ and $(x,y,z)_{\text{SPECT}}$ are the coarsely transformed and the original coordinates of the SPECT data, $(\overline{x},\overline{y},\overline{z})_{\text{SPECT}}$ and $(\overline{x},\overline{y},\overline{z})_{\text{CT}}$ are the mean values of the SPECT and CT set, $(V_x,V_y,V_z)^{\text{SPECT}}$ and $(V_x,V_y,V_z)^{\text{CT}}$ are the voxel sizes of the SPECT and CT data, respectively.

The final step of the preprocessing consists of the production of the distance map from the CT surface, DM(CT). The distance map is a discrete space where each voxel holds a value equal to its Euclidean distance from the closest node of the CT inner skull surface.[13] The distance map accelerates the process of matching two surfaces consisting of N nodes each, since it reduces the problem's complexity from $O(N^2)$ to $O(N)$. In the Appendix, a fast implementation of the 3-D Euclidean distance transformation is presented in pseudocode.

Volume-based automatic registration: Normally, no preprocessing for the extraction of common anatomical structures (such as surfaces) is necessary for this technique, except for the coarse preregistration, as it has been described in the previous paragraph. However, while the application of the volume-based automatic registration method produces very accurate matches of the brain structures, it tends to expand the SPECT image slightly outside the inner skull surface, as it was shown during this study.[29] For this reason, it was decided to apply the preprocessing step of removal of the skull from the CT data. The skull extraction process is defined as follows:

$$E_{\text{CT}} = X \times [T(X) \circ B], \tag{4}$$

where E_{CT} is the resulting gray level CT data with the bone structure removed, X is the original CT data (gray values), $T(X)$ is the threshold operator that produces a binary output such that voxels with original values greater than the threshold level obtain values equal to 1, $\circ$ is the symbol for the opening operation (erosion followed by a dilation) using the circular disk B with a diameter of 21 pixels, as a structuring element. The erosion operation causes the binary skull and any outside structure to disappear, while the dilation operation restores the remaining binary brain structure to its original size. The symbol $\times$ denotes the element-by-element multiplication operator, implementing a masking operation. The CT skull extraction process is clearly demonstrated in Fig. 2. Figure 2(a) shows the original CT slice 14 of the Pair-4, Fig. 2(b) the result of the application of the threshold operation, $T(X)$, to produce a binary image, Fig. 2(c) is the result of the opening operation onto the binary image that removes all the background pixels along with the bone structure, and finally in Fig. 2(d) the corresponding CT image without any bone structure, extracted according to Eq. (4) is displayed.

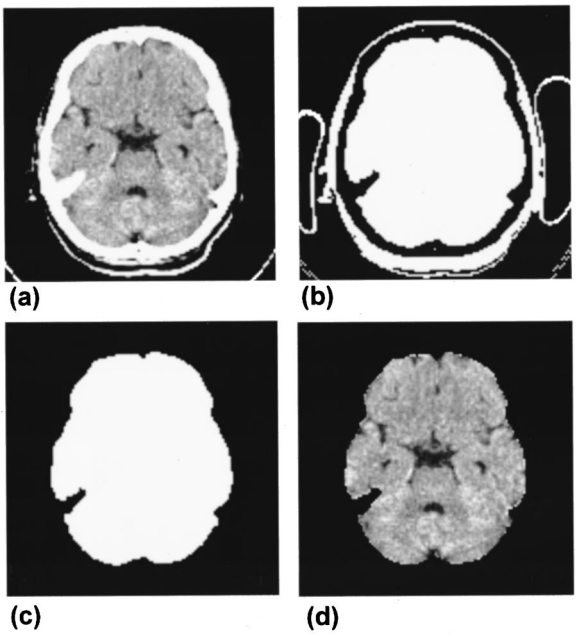

FIG. 2. (a) Transverse slice 14 from the original CT data of Pair-4. (b) The result of the application of the threshold operation, $T(X)$, to produce a binary image. (c) The result of the opening operation onto the binary image, which removes all the background along with the bone structure while it restores the brain CT area to its original size. (d) The corresponding CT slice with the skull structure removed.

The measure of match (MOM)

After the preprocessing of the CT and the SPECT data, the registration proceeds by optimizing the function of measure of match, over the parameters of the selected geometric transformation model.

Surface-based automatic registration: The measure of match (MOM) is defined as the average Euclidean distance between the CT and SPECT surfaces. It can be mathematically expressed as follows:

$$\text{MOM} = \frac{1}{n} \sum_{i:\text{SPECT}(x,y,z)_i \neq 0} \text{DM}_{\text{CT}}(x',y',z')_i, \tag{5}$$

where

$$(x',y',z')=[T_x(x,y,z),T_y(x,y,z),T_z(x,y,z)], \quad (6)$$

where DM_{CT} denotes the distance map produced by the CT inner skull surface, $(x,y,z)_i$ are voxels that lie on the SPECT outer brain surface, T_x, T_y, and T_z are the transformations for the *x*, *y*, and *z* coordinates, and *n* is the number of voxels of the SPECT surface. The MOM has to be minimized, requiring the SPECT surface to be transformed in such a way that it lies on low value voxels of the distance map produced by the CT surface, or equivalently to overlap with the CT surface.

Volume-based automatic registration: The MOM that is employed for this method is the mutual information (MI) or relative entropy of the two images to be registered. This is a measure of the combined information of the two images, defined as

$$\mathrm{MI}=\sum_{\mathrm{CT,SPECT}} p(\mathrm{CT,SPECT})\log\frac{p(\mathrm{CT,SPECT})}{p(\mathrm{CT})p(\mathrm{SPECT})}, \quad (7)$$

where $p(I)$ is the probability distribution of image I and $p(\mathrm{CT,SPECT})$ is the joint probability distribution of CT and SPECT images. In more specific terms,

$$p(i,j)=p[\mathrm{CT}(x,y,z)=i|\mathrm{SPECT}(x,y,z)=j],\forall(x,y,z) \in \mathrm{CT}\cap\mathrm{SPECT}, \quad (8)$$

where $p(i,j)$ is the probability of any voxel (*x*,*y*,*z*) of the CT data having value *i*, given that the same voxel (*x*,*y*,*z*) of the SPECT data has value *j*. This quantity is defined for all voxels that belong in the volumes of the CT and SPECT data that overlap (thus the intersection operator, $\cap$). The greater the value of MI, the better the match between the two images.

The geometric transformation model

The transformation model employed in the proposed registration methods is the affine transformation model, defined over a wide range of values to achieve robustness.[2] This transformation was employed to partially compensate any geometric transformation occurred in the SPECT data.[39] The affine transformation can be decomposed into a linear transformation and a simple translation. It can be shown that this transformation maps straight lines into straight lines, whereas it preserves parallelism between lines. In the 3-D case, it can be mathematically expressed as follows:

$$\begin{pmatrix} x' \\ y' \\ z' \end{pmatrix} = \begin{pmatrix} a_1 & a_2 & a_3 \\ b_1 & b_2 & b_3 \\ c_1 & c_2 & c_3 \end{pmatrix} \begin{pmatrix} x \\ y \\ z \end{pmatrix} + \begin{pmatrix} dx \\ dy \\ dz \end{pmatrix}. \quad (9)$$

The affine transformation is completely defined for the 3-D case by 12 independent parameters: (a_i,b_i,c_i) for $i=1, 2, 3$ and *dx*, *dy*, and *dz*.

The optimization technique

If the measure of match has multiple local minima, presents discontinuities or cannot be expressed analytically, a brute force-based exhaustive search is the only method that guarantees successful estimation of the parameter values. An exhaustive search in the case of an affine transformation model in order to register remote sensing images was proposed by Fuh *et al.*,[40] assuming that some of the unknown parameters can be estimated one at a time, in a serial manner, thus converting the multidimensional search into a sequence of optimization problems of lower dimensionality. Under this assumption, the authors were forced to narrow the range of the parameters in order to accelerate the execution of the program. However, in cases of nontrivial transformations with many independent parameters, an exhaustive search is not possible.

The measure of match that has been adopted in Eqs. (5) and (6) is nonlinear; therefore global optimization techniques are good candidates to explore the search space and estimate the unknown transformation parameters. The most efficient and attractive solution for search methods using nontrivial transformations is based on global optimization techniques such as simulated annealing (SA)[41] and genetic algorithms (GAs).[42,43] In Matsopoulos *et al.*[44] these two global optimization techniques and the Downhill Simplex Method (DSM),[45] as a standard one, were investigated in order to register retinal images. It was shown in the same study that GAs outperformed consistently and substantially the two other optimization techniques, independently of geometrical transformations or clinical data.

The definition of 12 independent parameters, combined with the presence of multiple local minima of the MOM (objective function), necessitates the use of GAs, as a global optimization technique, for the 3-D registration case, in conjunction with the affine transformation model, as an automatic registration method.

The GA operate with a population of solutions (also called individuals or offspring) of the optimization problem. A solution consists of the values of the parameters that are to be estimated. In this implementation, the values of the parameters are encoded in the solutions unaltered, as real values. Each population forms a generation. Initially (first generation), the solutions are created randomly, since we are using no *a-priori* knowledge about the specific problem. The GAs allow the solutions to interact through two main operators: crossover and mutation. The probability of two solutions performing crossover is an important parameter of the GAs optimization system, as it is the probability of mutation during crossover. In the specific implementation, the value of the probability of mutation has been encoded in the solution, rather than being kept constant. The process of selection is responsible for selecting the solutions that undergo the crossover operator.

The new generation that is produced by the action of the two operators on the previous generation replaces the previous one, and this process is continuous until a total number of generations is reached or a total number of function evaluations has been achieved. Since the selection process selects only the best solutions with respect to the objective function, statistically the next generations achieve better optimization of the MOM than the previous ones.

GAs hybridization with local optimization techniques is

not an unusual practice, mainly due to the GAs inefficiency to estimate the global optimum exact position, despite their ability to locate it approximately. Often, the GAs achieve convergence at a point of the search space very close to the location of the global optimum, whereas the lack of diversity of the population at the advanced stages of the search makes it either very time consuming or impossible to locate the exact position and value of the optimum. In these cases, bibliography extensively advises the use of a local optimization, which commences after the end of the genetic optimization and uses as an initial guess the best solution achieved so far by the GAs. The Powell conjugate gradient method was selected for the implementation of the hybrid scheme.[12]

The specific GAs hybrid system with a Powell technique that was implemented for this application can be summarized in the following pseudocode:

initialize the first generation of *n* individuals randomly
while (termination_condition is false) {
  decode and calculate the objective function of the *n* individuals
  select *N*/2 pairs of individuals
  apply crossover and mutation operator to produce *N* offspring
  replace the current generation by the *N* offspring
}
  locate the best solution achieved during the genetic evolution
  initiate multidimensional Powell method, using the best solution as an initial guess.

IMPLEMENTATION DETAILS OF TWO REGISTRATION ALGORITHMS

The registration scheme proposed in the paper has been developed by the authors. More specifically, the algorithms related to the registration processes, including the transformation algorithm, the optimization process, and the surface triangulation method, have been developed in $C++$, whereas the rendering process has been performed by a standard VRML viewer. Furthermore, the development and the evaluation of the compared registration methods have been performed on a Unix workstation (SGI workstation with 128 MB and high impact graphics), which was dedicated for the specific study.

Implementation details of the transformation model

Throughout this study, the affine transformation model has been considered for the registration of CT–SPECT brain images. The allowed ranges of the parameters of Eq. (9) are determined during the experimental phase for both registration methods and are presented. These values cover the majority of the brain image pairs and can be redefined by the user in situations where extreme transformation is required:

a_1,b_2,c_3	$[0.9,1.1]$
a_2,a_3,b_1,b_3,c_1,c_2	$[-0.3,0.3]$
dx,dy	$[-40,40]$
dz	$[-20,20]$

It can be observed that in the affine transformation, the parameters controlling the contribution of x coordinate to the transformed x' coordinate, the contribution of y coordinate to the transformed y' coordinate, and the contribution of z coordinate to the transformed z' coordinate, (a_1,b_2,c_3), are symmetrically kept in the range (1 ± 0.1). Also, the parameters controlling the contribution of the x to the transformed y and z coordinate, the contribution of the y to the transformed x and z coordinate, the contribution of the z to the transformed x and y coordinate, $(a_2,a_3,b_1,b_3,c_1,c_2)$, are symmetrically kept in the range (±0.3). The translation parameters, (dx,dy) and (dz), are kept within the range $[-40,40]$ and $[-20,20]$, respectively.

Implementation of the optimization technique

In this study, GAs are combined with the Powell method, for the estimation of the values of the affine transformation parameters. The details of the implementation of GAs and the Powell method are summarized as follows:

Population	100
Number of generations	100
Total number of function evaluations	10,000
Probability of crossover	1.0
Probability of mutation/ parameter	0.01–0.1 encoded into the individual
Parameter encoding	real values
Selection	tournament selection
Type of crossover	linear and arithmetic
Hybridization	Powell at the end of GAs optimization
First generation	uniformly random

QUANTITATIVE ANALYSIS

In order to quantitatively compare the accuracy and efficiency of the two proposed methods, a validation method must be selected. In this study, the lack of fiducial skin markers, due to the nature of clinical protocol, does not allow comparisons against the marker-based approach, which is widely accepted as a golden standard in registering medical data from other modalities (CT and MR).[4] Also, the well-established Target Registration Error (TRE), according to West *et al.*,[30] could not be applied in this case since the medical experts were not in a position to accurately place landmarks in the SPECT image, by means of software, after the acquisition, due to the low spatial resolution of the data. The comparison between the two proposed registration methods will therefore take place using either their own MOM or other unbiased image similarity criteria. Nevertheless, we performed various tests using our algorithms on registering CT-MRI data, which have been available to us according to the international project entitled ''Evaluation of retrospective image registration,'' sponsored by the National Institute of Neurological Disorders and Stroke, Project No. 1 R01 NS33926-02, with principal investigator Professor J. Michael Fitzpatrick). The obtained results have been sent for evaluation to the authors of Ref. 30 according to the strict

procedures that have been defined within the aforementioned web-based project (http://cswww.vuse.vanderbilt.edu/~image/registration/).

As it can be seen from the definition of the MOMs that are used in the proposed methods [Eq. (5) and Eq. (7)], the surface-based method uses the average distance of two surfaces, whereas the volume-based method uses the mutual information (MI) criterion, which is a pure number. The two MOMs (mutual information—MI—and average surface distance) are used as modules of the registration schemes (volume-based and surface-based methods, respectively), in the sense that the optimization process is using these MOMs to estimate the unknown transformation parameters. Thus, the two proposed methods do not employ directly comparable MOMs. Evaluating the volume-based method using the average surface distance, or calculating the MI criterion of the result of the surface-based method would be biased, since, in the first case, the volume-based was not designed to minimize the average surface distance, or *vice versa*.

The appropriate approach would be to employ an image similarity measure and calculate its value for the resulting registered images of both methods. Ideally, this independent measure of match (MOM) should be of a different nature from both MOMs that are being examined.

In this specific case, a number of image similarity criteria have been investigated. The normalized cross-correlation coefficient,[46] the gradient correlation coefficient,[47] and similarity measures, based on the difference image,[48] are the most widely used. The similarity measures based on the difference images are not applicable in the case of registering CT and SPECT images due to its operation, which can only take place for intramodality registration. Therefore, the normalized cross correlation was finally selected. Its mathematical definition is given below:

$$cc=\frac{\Sigma_{(i,j)\in A}[I_{\mathrm{CT}}(i,j,k)-\overline{I}_{\mathrm{CT}}][I_{\mathrm{SPECT}}(i,j,k)-\overline{I}_{\mathrm{SPECT}}]}{\sqrt{\Sigma_{(i,j)\in A}[I_{\mathrm{CT}}(i,j,k)-\overline{I}_{\mathrm{CT}}]^2\Sigma_{(i,j)\in A}[I_{\mathrm{SPECT}}(i,j,k)-\overline{I}_{\mathrm{SPECT}}]^2}}, \tag{10}$$

where $\overline{I}_{\mathrm{CT}}$, $\overline{I}_{\mathrm{SPECT}}$ are the mean values of the image at the overlap region of the CT and SPECT, $(i,j,k)\in A=\mathrm{CT}\cap\mathrm{SPECT}$. The normalized cross-correlation's value ranges between -1 (least similar) to $+1$ (most similar). It must be pointed out that the two proposed methods are also compared against a well-established registration method, the Iterative Closest Point (ICP) method. The three registration methods were evaluated for all five pairs of data.

EXPERIMENTAL RESULTS

Quantitative results

In Table II, the normalized cross-correlation values of the registration using the surface- and the volume-based methods against the ICP are presented.

In order to assess if there is a difference of the correlation coefficient between the three registration methods, a one-way repeated-measures analysis of variance (RM-ANOVA) is performed.[49] The null hypothesis is that the independent variable (i.e., the registration method) has no effect on the estimation of the correlation coefficient. The results of the test are listed in Table III. The first column of the table presents the source of variation of the correlation coefficient. One source of variation is the independent variable manipulation (registration method): five of the estimations were obtained using the volume-based method, five using the surface-based method, and five using the ICP method. Another source of variation is the individual differences: the mean value of the three correlation coefficients corresponding, for example, to the Pair-1 is likely to be different than that corresponding to the Pair-3. The final component of the total variability is due to the so-called registration method $\times$pairs interaction and it describes how the patterns of the correlation coefficient are affected by the levels of the independent variable (registration method). The quantification of the various sources of variation is achieved by the use of the sum of squares (SS), which is an abbreviation for the ''sum of the squared deviations from the mean.'' The values for the sum of squares for the three components are listed in the

TABLE II. Quantitative results of the three registration methods: the surface-based, the volume-based, and the ICP method using the normalized cross correlation, as a similarity criterion, for all CT–SPECT image pairs.

	Correlation coefficient value		
Data pairs	Volume-based	Surface-based	ICP
1	0.474	0.4196	0.423
2	0.424	0.408	0.397
3	0.506	0.3013	0.402
4	0.407	0.331	0.337
5	0.46	0.44	0.423
Average	0.454	0.380	0.396
Std. deviation	0.0395	0.0603	0.0353

TABLE III. One-way repeated measures—ANOVA for assessing if the mean values of the correlation coefficient are different between the three algorithms

Source of Variation	SS	df	MS	F	p value
Registration method (RM)	0.015 198 4	2	0.0076	4.968	0.0396
Pairs (P)	0.013 533 8	4	0.003 383		
(RM)$\times$(P) (residual)	0.012 237 1	8	0.001 530		
Total	0.040 969 3	14			

TABLE IV. *p* values of a Newman–Keuls multiple comparison test for assessing if the values of the correlation coefficient are different for the methods under comparison

Methods under comparison	*p* value
Mutual distance	<0.05
Mutual ICP	<0.05
Distance ICP	>0.05

second column of the Table III. The third column of the table contains the degrees of freedom (df) for each source of variation. The column labeled as MS presents the mean of squares, which is the ratio of the sum of squares to the degrees of freedom. Since the mean of squares corresponding to the second component of variation is not used for further calculations, it is not necessary to include it in Table III. The systematic effect of the registration method on the value of the correlation coefficient is quantified by the so-called *F* ratio, which is the ratio of the mean squares of the first component of variation to the mean of squares of the third component of variation. The *p* value corresponding to the computed *F* ratio (0.039 578 3) indicates that the null hypothesis can be rejected with significance level 0.05, i.e., the registration method has a significant effect on the value of the correlation coefficient.

Furthermore, a post hoc analysis is performed in order to determine between which registration methods there is a significant difference of the correlation coefficient. In Table IV, the results of the Newman–Keuls multiple comparison test between all the possible combinations of registration methods are listed. The null hypothesis is that the two methods under consideration do not differ as per the correlation coefficient.

As can be observed, there is a significant statistical difference of the values of the correlation coefficient between the volume-based method and both the surface-based and the ICP method. In particular, the correlation coefficient obtained by the volume-based method is higher than that of the surface-based and the ICP method, thus the volume-based method systematically outperforms the other two methods. On the contrary, there is not a statistical difference of the value of the correlation coefficient between the surface-based and the ICP methods.

Qualitative results

In Fig. 3, the pre- and post-registered SPECT outer brain surfaces are rendered in the CT coordination system, along with the inner skull CT surface, using a standard VRML 2.0 browser. The technique used for rendering is a surface rendering technique, where the red surface corresponds to the inner CT skull surface and the blue surface corresponds to the SPECT brain surface. The SPECT brain surface is rendered with transparency, therefore, wherever it lies outside the CT surface, it is rendered with a purple color, whereas when it lies inside the CT surface it is hidden by it. Successful registration results in areas of the SPECT surface that rapidly interchange with the CT skull surface. A degree of spatial misalignment occurs between the preregistered SPECT and CT surfaces in Fig. 3(a), especially in the parieto-occipital and the iniac areas. This misalignment is finally corrected by the application of the proposed volume-based automatic registration method, in Fig. 3(b), where the registered SPECT surface is closely aligned with the inner skull CT surface. Areas of seemingly imperfect alignment can be attributed to the segmentation of the skull structure.

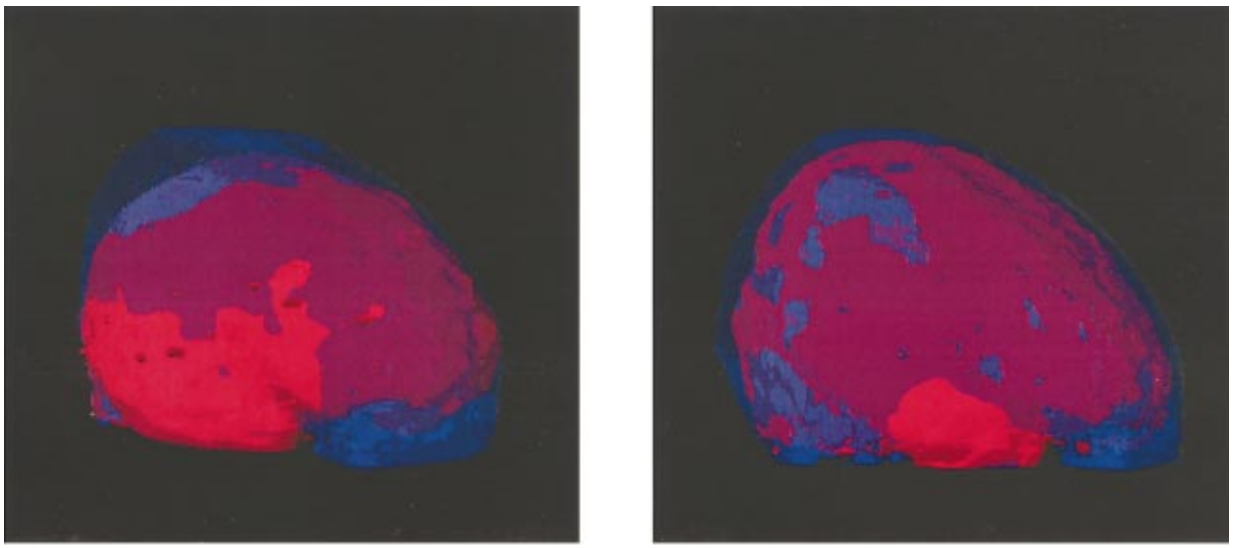

FIG. 3. Visual assessment of the volume-based automatic registration method by superposing the SPECT surface on the corresponding CT surface for the Pair-4, before (a) and after (b) the proposed registration method.

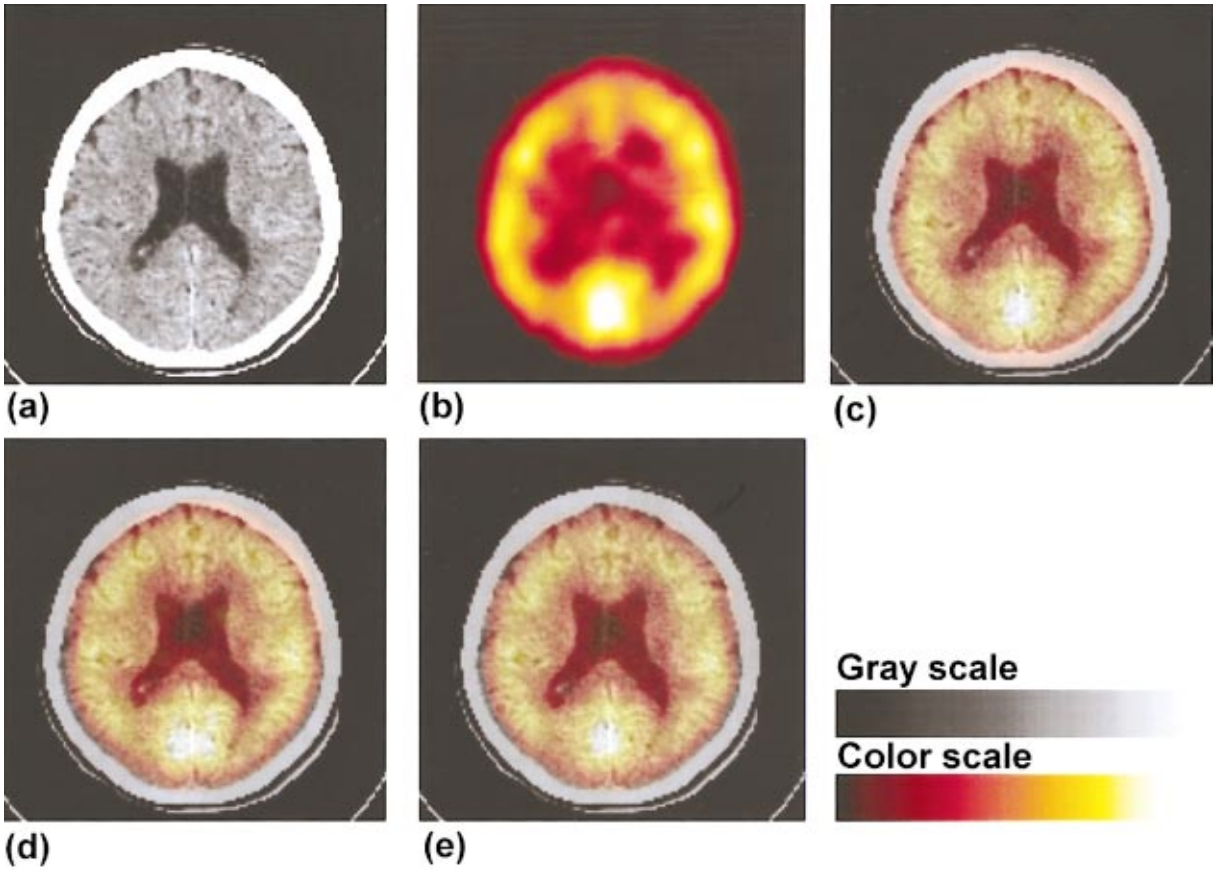

FIG. 4. Original CT transverse slice 35—enhanced for visibility (a). Corresponding SPECT slice (b). CT transverse slice fused with the corresponding slice from the registered SPECT data, using the MI method (c). CT slice fused with the registered SPECT data using the surface-based method (d). CT slice fused with the registered SPECT data using the ICP method (e).

The performance of the surface- and the volume-based automatic registration methods is also visually compared against the ICP method for data of Pair-4, which was selected as the most representative according to the team of experts. Furthermore, the internal SPECT anatomical structure was more evident in this pair, probably due to pathology, thus making the task of qualitative evaluation of the techniques easier. In Figs. 4 and 5, selected regions of the registered SPECT slices of Pair-4 are superimposed on the corresponding CT transverse slices 35 and 17, respectively. To enhance the visual assessment of the registration methods, the SPECT data have been displayed using pseudocolor, specifically the hot body color map, as indicated in the figures. A pseudocolor map defines the correspondence between a gray value and an (R,G,B) triplet, thus producing the effect of color display from noncolor information. The correspondence between the gray scale and the color map is indicated in Figs. 4, 5, and 6. The hot body color map is defined by psychophysiologic criteria and it has been considered as very appropriate for the display of SPECT data.[39] The selection of the particular slices presented in the figures was based on the amount of internal structure that is visible on the SPECT images, such as ventricles and ischemic pathologies. As it can be observed in Fig. 4, the volume-based registration (MI) method achieves superior continuity regarding the internal brain structures, such as the lateral ventricles and the left occipital horn. The lowest degree of continuity is achieved by the ICP method, whereas the surface-based method lies in the middle. This can be explained, since the MI is the only criterion in this study that takes into consideration the information from the interior of the two modalities, indicating spatial alignment of corresponding structures of the two images that are to be registered. The criteria employed by the surface-based method or the ICP rely on the surface information, ignoring the spatial alignment of internal structures. The superiority of volume-based registration techniques over surface-based ones because of the nature of the employed measure of match has been reported.[31] The ICP method has either produced a set of unrealistic transformation parameters for the specific pair of datasets or it may have miscalculated the z displacement, since the degree of discontinuity between the CT and SPECT internal structure is much greater than that of the surface-based method. The inner skull CT surface and the outer SPECT brain surface present a high degree of continuity regarding the ICP method, as well as with the volume-based registration method. The surface-based method presented only few local discrepancies.

Results from transverse CT slice 17 of Pair-4 also support the above findings, although brain structure at this level is not as easily identifiable (Fig. 5).

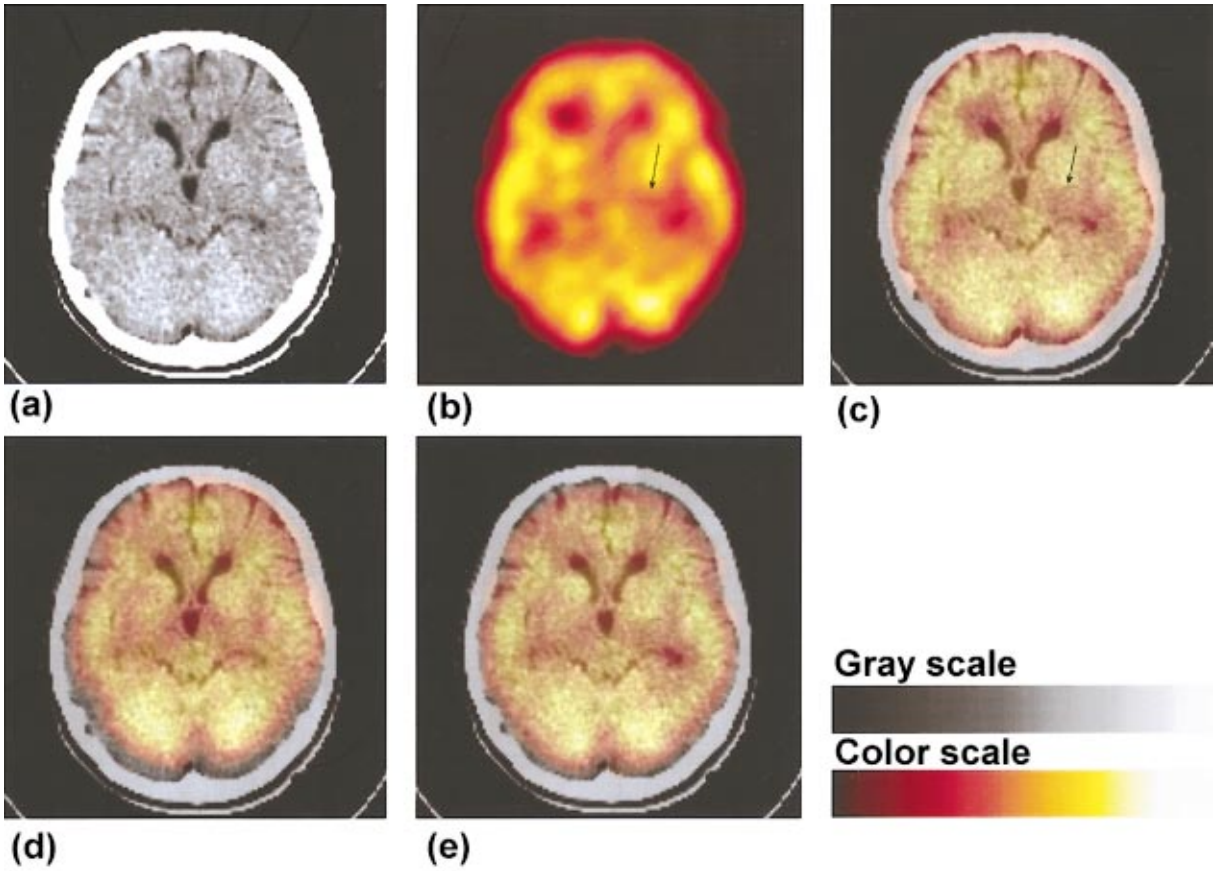

FIG. 5. Original CT transverse slice 17—enhanced for visibility (a). Corresponding SPECT slice (an arrow indicates the ischemia in the left posterior limb of the internal capsule) (b). The CT transverse slice fused with the corresponding slice from the registered SPECT data, using the MI method (an arrow indicates the ischemia in the left posterior limb of the internal capsule) (c). CT slice fused with the registered SPECT data using the surface-based method (d). CT slice fused with the registered SPECT data using the ICP method (e).

DISCUSSION

Surface- and a volume-based automatic registration methods have been proposed in this paper for matching CT and SPECT data of the human brain under a clinical protocol. For the determination of the parameters of the geometric transformation, the optimization technique of genetic algorithms was used. Using independent MOM criteria we showed that the volume-based method consistently outperforms the surface-based method.

Since the SPECT study is a brain perfusion study, bone structure (such as the skull) cannot be imaged by SPECT. Therefore, in registering CT and SPECT datasets, the outer limits of the brain tissue, as imaged by SPECT, should coincide with the inner skull, as imaged by CT. Thus, a preprocessing step to extract the inner skull CT surface and the outer SPECT surface has been applied for the surface-based registration method. Furthermore, a preprocessing step of removal of the skull from the CT data has been required prior to the volume-based registration.

Figure 6 demonstrates the necessity of this preprocessing step before applying the volume-based registration method. Figure 6(a) shows the transverse fused slice 35 (selected regions of the SPECT data, superimposed on the CT data) without applying the skull-removal preprocessing step on the CT data, whereas Fig. 6(b) shows the same fused results, after applying the skull-removal preprocessing step on the CT data. It can be observed that in the first case the registered SPECT areas invade the CT skull surface, thus deteriorating the performance of this method significantly. The performance is improved, as can be seen in Fig. 6(b), by the application of the aforementioned preprocessing step. This improvement is not due to different spatial resolution of the two imaging modalities, because (a) the voxel size of the two modalities has been taken into consideration [in Eq. (3)], (b) the effect appears only in the volume-based registration technique and could be attributed to the properties of the mutual information criterion, and (c) the effect disappears after the removal of the skull from the CT data, prior to the volume-based registration process.

One further disadvantage of the surface-based registration method is the necessity of identification of common anatomical structures to be matched in both modalities; inaccuracies are inevitably introduced during this process. These inaccuracies of the surface-based registration method are due to the difficulty of obtaining the SPECT brain surface. The alignment of the internal structures may be affected by the registration of the extracted surfaces. In order to quantitatively evaluate the performance of the surface-based registration

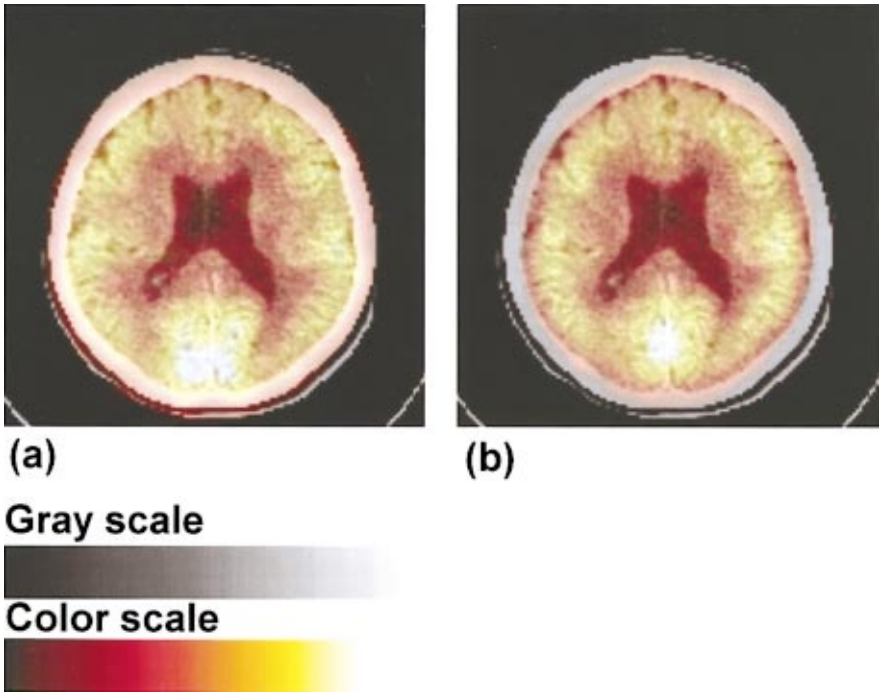

FIG. 6. CT transverse slice fused with the corresponding slice from the registered SPECT data, using the MI method, without removing the CT bone structure (a). The same fused slice, using the volume-based method (MI), after performing the CT bone structure removal preprocessing step (b).

method, in terms of determination of the SPECT brain surface, a study was also performed.

According to this study, the actual SPECT brain surface has been obtained using a threshold operator as described in the preprocessing section. As it can be seen in Fig. 7, the optimum threshold level is difficult to be determined for the SPECT data, whereas the determination of the threshold value for the CT is a simpler process, as indicated by the higher slope of the line profiles. Thus, the inaccurate determination of the SPECT brain surface may introduce inaccuracies during the application of the surface-based method. These inaccuracies are quantified in Fig. 8, where the average brain SPECT-CT inner skull distance is plotted in millimeters against different SPECT threshold values, for Pair-4. The average brain SPECT-CT inner skull distance has been calculated for each threshold value according to the algorithm presented in the Appendix, using the surface-based registration technique. This measure of match was selected because the average surface distance is associated with the automatic surface-based registration technique and this specific technique was the one affected by these kinds of inaccuracies. As it can be observed, there is an area round the threshold level of 10 where the automatic surface-based registration technique produces the most accurate performance. Its performance deteriorates rapidly as the threshold level increases above 15. Similar observations were recorded for the rest of the pairs.

Additionally, the volume-based method does not suffer from the aforementioned disadvantage, despite the fact that a preprocessing step toward removal of the CT bone structure was needed. Furthermore, as it was pointed out above, the bone structure in the CT data is well defined and thus easily segmented. This method, however, does not require the iden-

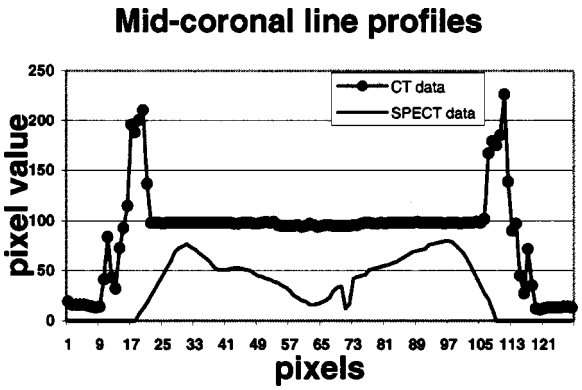

FIG. 7. Mid-coronal line profiles of a CT transverse slice and the corresponding (registered) SPECT slice.

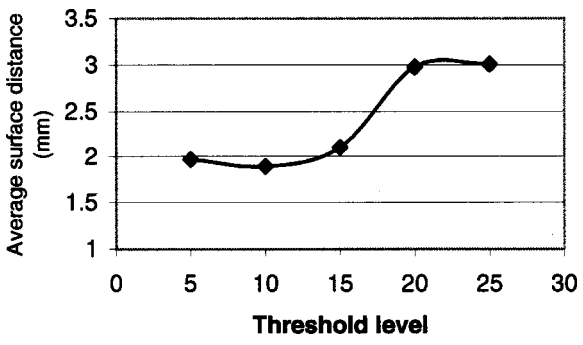

FIG. 8. Performance of the automatic surface-based registration method against the determination of the brain SPECT surface (in terms of threshold level) for the Pair-4.

tification of the corresponding SPECT brain surface, which cannot be unambiguously identified and therefore is the source of spatial inaccuracies.

The ICP algorithm suffers from similar to the surface-based method's disadvantage; it does not require the definition of common anatomical structures, such as surfaces, but it does require the identification of homologous points between the two images that are to be registered. In the specific case of registering CT and SPECT brain images, most of the points used for the registration of the images lay on the surfaces used by the surface-based registration method. This explains the fact that the quantitative results of Table II do not show any statistical difference between the two methods.

Finally, the performance of the surface- and volume-based registration methods shows no correlation with the voxel size within the range of sizes given in Table I. Nevertheless, realigning CT and MRI data, the performance of the automatic surface-based registration method deteriorated as the voxel size increases to values outside of the range of the current study, as it was described in the work of Matsopoulos *et al.*[10]

CONCLUSIONS

A volume-based registration using the MI criterion, in conjunction with genetic algorithms and the Powel method, has been successfully applied to automatically register five pairs of CT and SPECT data. The proposed method provides the clinicians with a registration tool characterized by stability and repeatability of performance, speed of execution, independence of clinical protocol, and robustness due to the employment of the genetic algorithms, as an optimization process. At the present study, the patients involved suffer from ischemia (acute–chronic–transient) and from subarachnoid hemorrhage. It is well known that in brain ischemia SPECT is able to provide an early diagnosis, while CT better describes the anatomic features.

In the near feature, the current study will be enhanced with more clinical trials and a new clinical protocol is going to be established involving also patients suffering from brain tumors, since CT data provides finer anatomical details while the corresponding SPECT data successfully delineate the edges of the malignancy. Registering the two data will provide the clinical experts with information to estimate more accurately the extent and the position of the lesion, thus resulting in a more accurate diagnosis, prognosis and consequent treatment.

APPENDIX: FAST IMPLEMENTATION OF 3-D EUCLIDEAN DISTANCE TRANSFORMATION

The distance transformation (DT) accepts as input a binary image (e.g., a given surface marked as nonzero voxels) and produces as output a 3-D float image, each voxel of which holds the distance of the specific voxel from the closest nonzero voxel of the input image. The resulting float image is called the distance map (DM). Several implementations of DT exist in the bibliography.[13] The adopted implementation is very fast, compared to the other implementations, and is based on a list. Each voxel of the resulting distance map is associated with a closest voxel from the binary input image. This information is stored into a lookup table, which greatly accelerates execution time, with manageable memory requirements. The algorithm for DT can be summarized in the pseudocode as follows:

Insert all voxels of the given surface into the list,
initialize the lookup table (set distances to an unused label),
for all surface voxels, set the closest voxel as the same voxel,
while (list not empty),
extract the top voxel from the list, set this as the current voxel, expand its six closest neighbors (in three dimensions) and insert them at the end of the list,
calculate the minimum distance min_dist, of each of the six neighbors from the closest voxel of the current voxel,
if min_dist is less than the distance of the neighbor point from the already assigned closest voxel to it, then
set the closest voxel of the neighbor equal to the closest voxel of the current voxel (update the lookup table).

[a]Electronic mail: kagadis@med.upatras.gr
[b]Author to whom correspondence should be addressed; electronic mail: gnikif@med.upatras.gr

[1] R. Bajcsy and S. Kovacic, "Multiresolution elastic matching," Comput. Vis. Image Underst. **46**, 1–29 (1989).
[2] P. A. van den Elsen, E. J. Pol, and M. A. Viergever, "Medical image matching: A review with classification," IEEE Eng. Med. Biol. Mag. **12**, 26–39 (1993).
[3] C. R. Maurer, Jr. and J. M. Fitzpatrick, "A review of medical image registration," in *Interactive Image Guided Neurosurgery*, edited by R. J. Maciunas (American Association of Neurological Surgeons, Park Ridge, IL, 1993), pp. 17–49.
[4] C. R. Maurer, Jr., J. M. Fitzpatrick, M. Y. Wang, R. L. Galloway, R. J. Maciunas, and G. G. Allen, "Registration of head volume images using implentable fiducial markers," IEEE Trans. Med. Imaging **16**, 447–462 (1997).
[5] V. Mongioj, A. Brusa, G. Loi, E. Pignoli, A. Gramanglia, M. Scorsetti, E. Bombardieri, and R. Marchesini, "Accuracy evaluation of fusion of CT, MR, and SPECT images using commercially available software packages (SRS PLATO with IFS)," Int. J. Radiat. Oncol., Biol., Phys. **43**, 227–234 (1999).
[6] D. L. G. Hill, D. J. Hawkes, J. E. Crossman, M. J. Gleeson, T. C. S. Cox, E. E. Bracey, A. J. Strong, and P. Graves, "Registration of MR and CT images for skull base surgery using point-like anatomical features," Br. J. Radiol. **64**, 1030–1035 (1991).
[7] D. L. G. Hill, P. G. Batchelor, M. Holden, and D. J. Hawkes, "Medical image registration," Phys. Med. Biol. **46**, R1–R45 (2001).
[8] D. J. Hawkes, D. L. G. Hill, and E. C. M. L. Bracey, "Multi-modal data fusion to combine anatomical and physiological information in the head and the heart," in *Reiber JHC*, Cardiovascular Nuclear Medicine and MRI, edited by E. E. Van der Wall EE (Kluwer Academic, Dordrecht, The Netherlands, 1990), pp. 113–130.
[9] P. Clarysse, J. Rousseau, D. Gibon, S. Blond, C. Vasseur, and X. Marchandise, "A computer-assisted system for 3-D frameless localization in stereotaxic MRI," IEEE Trans. Med. Imaging **10**, 523–529 (1991).
[10] G. K. Matsopoulos, K. K. Delibasis, and N. A. Mouravliansky, "Medical image registration and fusion techniques: A review," in *Advanced Signal Processing Handbook*, edited by S. Stergiopoulos (CRC, New York, 2001), pp. 19.1–19.30.
[11] C. A. Pelizzari, G. T. Y. Chen, D. R. Spelbring, R. R. Weichselbaum, and C. T. Chen, "Accurate three-dimensional registration of CT, PET and/or MR images of the brain," J. Comput. Tomogr **13**, 20–26 (1989).
[12] W. Press, W. Vetterling, S. Teukolsky, and B. Flannery, *Numerical Recipes in C*, 2nd ed. (Cambridge University Press, Cambridge, 1992).
[13] D. Kozinska, O. J. Tretiak, J. Nissanov, and C. Ozturk, "Multidimensional alignment using the Euclidean distance transform," Graph. Models Image Process. **59**, 373–387 (1997).

[14] G. Borgefors, ''Hierarchical chamfer matching: A parametric edge matching algorithm,'' IEEE Trans. Pattern Anal. Mach. Intell. **10**, 849–865 (1988).
[15] M. Van Herk and H. M. Kooy, ''Automatic three-dimensional correlation of CT–CT, CT–MRI, and CT–SPECT using chamfer matching,'' Med. Phys. **21**, 1163–1178 (1994).
[16] M. Jiang, R. A. Robb, and K. J. Molton, ''A new approach to 3-D registration of multimodality medical image by surface matching,'' Proc. SPIE **1808**, 196–213 (1992).
[17] P. J. Besl and N. D. McKay, ''A method for registration of 3-D shapes,'' IEEE Trans. Pattern Anal. Mach. Intell. **14**, 239–256 (1992).
[18] A. Collignon, D. Vanderaeulen, P. Suetens, and G. Marshal, ''Registration of 3-D multimodality medical images using surfaces and point landmarks,'' Pattern Recogn. Lett. **15**, 461–467 (1994).
[19] C. R. Maurer, Jr., G. B. Aboutanos, B. M. Dawant, R. J. Maciunas, and J. M. Fitzpatrick, ''Registration of 3-D images using weighted geometrical features,'' IEEE Trans. Med. Imaging **15**, 836–849 (1996).
[20] J. Y. Chiang and B. J. Sullivan, ''Coincident bit counting—A new criterion for image registration,'' IEEE Trans. Med. Imaging **12**, 30–38 (1993).
[21] T. Radcliffe, R. Rajapekshe, and S. Shalev, ''Pseudocorrelation: A fast, robust, absolute, gray level image alignment algorithms,'' Med. Phys. **21**, 761–769 (1994).
[22] J. B. A. Maintz, P. A. van den Elsen, and M. A. Viergever, ''Comparison of feature based matching of CT and MR brain images,'' in *Computer Vision, Virtual Reality, and Robotics in Medicine*, edited by N. Ayache (Springer-Verlag, Berlin, 1995), pp. 219–228.
[23] J. B. A. Maintz, P. A. van den Elsen, and M. A. Viergever, ''Evaluation of ridge seeking operators for multimodality medical image matching,'' IEEE Trans. Pattern Anal. Mach. Intell. **18**, 353–365 (1996).
[24] P. A. Van den Elsen, J. B. A. Maintz, E. J. D. Pol, and M. N. Viergever, ''Automatic registration of CT and MR brain images using correlation of geometrical features,'' IEEE Trans. Med. Imaging **14**, 384–396 (1995).
[25] P. A. Van den Elsen, E. J. D. Pol, T. S. Sumanaweera, P. F. Hemler, S. Napel, and J. R. Adler, ''Grey value correlation techniques used for automatic matching of CT and MR brain and spine images,'' Proc. SPIE **2359**, 227–237 (1994).
[26] C. Studholme, D. L. G. Hill, and D. J. Hawkes, ''Automated registration of truncated MR and CT datasets of the head,'' *Proceedings of the British Machine Vision Conference*, September 1995, edited by David Pycock, Vol. 1, pp. 27–36.
[27] R. P. Woods, J. C. Mazziotta, and S. R. Cherry, ''MRI–PET registration with automated algorithm,'' J. Comput. Tomogr **17**, 536–546 (1993).
[28] A. Collignon, F. Maes, D. Delaere, D. Vandermeulen, P. Suetens, and G. Marshal, ''Automated multi-modality image registration based on information theory,'' in *Information Processing in Medical Imaging*, edited by Y. Bizais, C. Barillot, and R. Di Paola (Kluwer, Dordrecht, The Netherlands, 1995), pp. 263–274.
[29] F. Maes, A. Collignon, D. Vandermeulen, G. Marchal, and P. Suetens, ''Multimodality image registration by maximization of mutual information,'' IEEE Trans. Med. Imaging **16**, 187–198 (1997).
[30] J. West, J. M. Fitzpatrick, M. Y. Wang, B. M. Dawant, C. R. Maurer, Jr., R. M. Kessler, and R. J. Maciunas, ''Retrospective intermodality registration techniques for images of the head: Surface-based versus volume-based,'' IEEE Trans. Med. Imaging **18**, 144–150 (1999).
[31] A. Goshtasby, D. A. Tuner, and L. V. Ackerman, ''Matching tomographic slices for interpolation,'' IEEE Trans. Med. Imaging **11**, 507–616 (1992).
[32] S. Vallabhajosula, R. E. Zimmerman, M. Picard, P. Stritzke, I. Mena, R. S. Hellman, R. S. Tikofsky, M. G. Stabin, R. A. Morgan, and S. J. Goldsmith, ''Technetium-99m ECD: a new brain imaging agent: in vivo kinetics and biodistribution studies in normal human subjects,'' J. Nucl. Med. **30**, 599–604 (1989).
[33] F. Tanaka, D. Vines, T. Tsuchida, M. Freedman, and M. Ichise, ''Normal patterns on 99mTc-ECD brain SPECT scans in adults,'' J. Nucl. Med. **41**, 1456–1464 (2000).
[34] L. T. Chang, ''A method for attenuation correction in radionuclide computed tomography,'' IEEE Trans. Nucl. Sci. **25**, 638–643 (1978).
[35] American Association of Physicists in Medicine (AAPM) Report No. 6, ''Scintillation camera acceptance testing and performance evaluation,'' American Institute of Physics, 1980.
[36] American Association of Physicists in Medicine (AAPM) Report No. 22, ''Rotating scintillation camera SPECT acceptance testing and quality control,'' American Institute of Physics, 1987.
[37] American Association of Physicists in Medicine (AAPM) Report No. 39, ''Specification and acceptance testing of computed tomography scanners,'' American Institute of Physics, 1993.
[38] G. K. Matsopoulos and S. Marshall, ''Use of morphological image processing techniques for the measurement of a fetal head from ultrasound images,'' Pattern Recogn. **27**, 1317–1324 (1994).
[39] P. Sharp, P. Dendy, and W. Keyes, *Radionuclide Imaging Techniques* (Academic, New York, 1985).
[40] C. Fuh and P. Maragos, ''Motion displacement estimation using an affine model for image matching,'' Opt. Eng. **30**, 881–887 (1991).
[41] P. Van Laarhoven and E. Aarts, *Simulated Annealing: Theory and Applications* (D. Reidel Publishing, Dordrecht, 1987).
[42] D. Goldberg, *Genetic Algorithms in Optimization, Search and Machine Learning* (Addison-Wesley, New York, 1989).
[43] K. Delibasis, P. E. Undrill, and G. G. Cameron, ''Designing Fourier descriptor-based geometric models for object interpretation in medical images using genetic algorithms,'' Comput. Vis. Image Underst. **66**, 286–300 (1997).
[44] G. K. Matsopoulos, N. A. Mouravliansky, K. K. Delibasis, and K. S. Nikita, ''Automatic retinal image registration scheme using global optimization techniques,'' IEEE Trans. Inf. Technol. Biomed. **3**, 47–60 (1999).
[45] S. L. S. Jacoby, J. S. Kowalik, and J. T. Pizzo, *Iterative Methods for Nonlinear Optimization Problems* (Prentice–Hall, Englewood Cliffs, 1972).
[46] R. C. Gonzalez and R. E. Woods, *Digital Image Processing* (Addison-Wesley, New York, 1992).
[47] L. Lemieux, R. Jagoe, D. R. Fish, N. D. Kitchen, and D. G. T. Thomas, ''A patient-to-computed-tomography image registration method based on digitally reconstructed radiographs,'' Med. Phys. **21**, 1749–1760 (1994).
[48] G. P. Penney, J. Weese, J. A. Little, P. Desmedt, D. L. G. Hill, and D. J. Hawkes, ''A comparison of similarity measures for use in 2-D–3-D medical image registration,'' IEEE Trans. Med. Imaging **17**, 586–595 (1998).
[49] N. Furlong, E. Lovelace, and K. Lovelace, *Research Methods and Statistics: An Integrated Approach* (Harcourt Brace & Company, Orlando, 2000).